Combination of laser and radar altimeter height measurements to estimate snow depth during the 2004 Antarctic AMSR-E Sea Ice field campaign

Carlton J. Leuschen,[1] Robert N. Swift,[2] Josefino C. Comiso,[3] R. Keith Raney,[4] Rickey D. Chapman,[4] William B. Krabill,[2] and John G. Sonntag[2]

Received 13 April 2007; revised 3 December 2007; accepted 7 February 2008; published 1 April 2008.

[1] Among the most important parameters needed to evaluate the present and future state of Antarctic sea ice cover is the ice thickness. The retrieval of ice thickness using remote sensing techniques has been hampered by the absence of a capability to remotely measure snow thickness covering the sea ice. Data sets collected with Johns Hopkins Applied Physics Laboratory's Delay-Doppler Phase Monopulse (D2P) radar and NASA's Airborne Topographic Mapper (ATM) scanning lidar during NASA's Antarctic AMSR-E Sea Ice field campaign over the Bellingshausen Sea are used to demonstrate the potential of a remote-sensing technique for retrieval of snow cover thickness from an airborne platform. The technique takes advantage of the fact that the radar is most sensitive to the snow-ice interface while the lidar responds to the highly optically reflective snow surface. The difference between the radar- and laser-determined surfaces yields an estimate of snow thickness that appears to be reasonably consistent with expected values. The technique requires careful registration of the instrument footprints. Because there was no absolute range calibration of the lidar due to predeployment scheduling difficulties, the vertical offset between the instruments was resolved by determining the difference between measurements over leads. Elsewhere over sea ice the radar-defined surface is generally below the laser-defined surface consistent with the radar defining the snow-ice interface. Over a relatively small portion of the data, we observed opposite relationship between the sensor-defined surfaces for which we discuss a plausible physical explanation.

Citation: Leuschen, C. J., R. N. Swift, J. C. Comiso, R. K. Raney, R. D. Chapman, W. B. Krabill, and J. G. Sonntag (2008), Combination of laser and radar altimeter height measurements to estimate snow depth during the 2004 Antarctic AMSR-E Sea Ice field campaign, *J. Geophys. Res.*, *113*, C04S90, doi:10.1029/2007JC004285.

1. Introduction

[2] Sea ice accounts for roughly seven percent of the world ocean area and is considered a key component of the global climate system. Sea ice produces dense water that can initiate vertical convection [*Aagaard and Carmack*, 1989] or lead to the formation of bottom water that drives the global thermohaline circulation. Changes of this circulation may have a significant impact on the climate [*Rahmstorf*, 1997]. Sea ice moderates the ocean heat budget by acting as an insulating layer between the ocean and atmosphere. Sea ice has a high albedo and reflects much of the Sun's energy that would otherwise be absorbed. Reduction of sea ice will increase heat absorption into the ocean and will likely lead to increased melt driving the sea ice-albedo climate feedback mechanism [*Curry et al.*, 1995]. Such feedback mechanisms can potentially trigger a rapid climate change. Sea ice also has influences on global ecology and economy. Tiny pockets and channels of brine within the sea ice provide a habitat generally dominated by algae [*Smetacek and Nicol*, 2005], and the organic carbon produced within the ice is a major contributor to the primary production at high latitudes [*Wheeler et al.*, 1996; *Gosselin et al.*, 1997].

[3] The presence of snow cover on sea ice has a major influence on sea ice atmosphere interactions, the feedback effects on global climate, and the rate at which sea ice grows or declines [*Wu et al.*, 1999; *Fichefet and Morales Maqueda*, 1999; *Powell et al.*, 2005]. Snow has a very high albedo and very low thermal conductivity when compared to bare sea ice, which makes it a sensitive modeling parameter. The higher albedo reflects more of the incident sunlight and reduces the amount of heat absorbed by the underlying ice and ocean. The lower thermal conductivity

[1]Center for Remote Sensing of Ice Sheets, University of Kansas, Lawrence, Kansas, USA.
[2]Observational Science Branch, NASA Goddard Space Flight Center, Wallops Island, Virginia, USA.
[3]Cryospheric Sciences Branch, NASA Goddard Space Flight Center, Greenbelt, Maryland, USA.
[4]Applied Physics Laboratory, Johns Hopkins University, Laurel, Maryland, USA.

Copyright 2008 by the American Geophysical Union.
0148-0227/08/2007JC004285

increases the insulating effects and significantly reduces the amount of heat loss from the ocean and sea ice to the atmosphere. These effects indicate the necessity to include snow cover in sea ice modeling; however, the distribution and thickness of snow cover over large scales is still not well understood, and can vary quickly on Antarctic sea ice ranging from no cover at all to drifts greater than a meter in thickness within close proximity [*Massom et al.*, 2001].

[4] Remote sensing is the only feasible way to monitor sea ice on a global scale. Satellite observations of sea ice have been carried out with passive microwave sensors [*Comiso*, 2002; *Cavalieri et al.*, 2003], infrared imagery [*Lindsay and Rothrock*, 1995], optical imagery [*Nolin et al.*, 2002], synthetic aperture radar [*Kwok et al.*, 1992], and altimetry [*Laxon et al.*, 2003; *Kwok et al.*, 2004]. Satellite missions optimized for observation of cryospheric parameters, including that of sea ice, that are scheduled to be launched in the near future include the Cryosat-2 radar altimeter mission and possibly an ICESat laser altimeter follow-on mission.

[5] Conventional radar altimeters have been collecting data over the past 25 years. Additionally, improved radar altimeters such as the SIRAL on CryoSat are continuing to be developed to focus on the cryosphere. Both laser and radar altimeters offer their own specific benefits in terms of measurement accuracy, resolution, coverage, and lifespan. Comparisons between the measurements of these two instruments are essential for preserving the continuity of altimetry data over snow and ice, and also for providing the opportunity to extract additional data products through the combination and comparison of the measurements.

[6] A true measure of sea ice volume must include its thickness: a measurement that has continued to elude satellite and long-range airborne observations. Sea ice thickness can be indirectly estimated from satellite altimeter measurements of freeboard [*Laxon et al.*, 2003, *Kwok et al.*, 2004]. Monitoring sea ice thickness from orbit is attractive owing to the ability to provide regional and temporal coverage at scales appropriate to sample interannual variations. However, current methods to indirectly estimate sea ice thickness from orbital altimeter freeboard measurements either have poor spatial resolution or large errors due to unknown snow loading. Snow depth uncertainties introduce the largest error when converting freeboard to sea ice thickness for laser altimetry [*Kwok et al.*, 2004; *Giles et al.*, 2007].

2. Background

[7] A radar altimeter's response over ice is not always well understood, especially when there may be snow cover in the measurement footprint. Electromagnetic penetration of dry, cold snow is significant at radar frequencies [*Rignot et al.*, 2001, *Beaven et al.*, 1995]. More importantly, it is not yet fully understood what aspects of a radar waveform (which responds primarily to interfaces of large dielectric contrast, such as the top of the ice) may be compared to heights measured by a laser (which responds primarily to the upper optical surface at the top of the snow).

[8] Initial comparisons of coincidental and simultaneous laser and radar altimeter measurements were collected during a 2002 field campaign over Greenland, Svalbard, and Arctic sea ice [*Raney et al.*, 2003; *Raney and Leuschen*, 2003]. Data from some areas in the interior of Greenland showed a large offset, as much as 2 m, between the heights determined by the laser and the peak radar response. The radar showed a smaller return from the snow surface that was resolvable from the main peak response, which presumably is from the snow-ice interface. The laser provided coincident elevation measurements of the snow surface that agreed with the small radar response. We concluded that the radargram was resolving a surface layer due to snow accumulation. A major conclusion, other than mapping the accumulation layer, was that the radar is more sensitive to the lower snow-ice interface while the laser only responds to the snow-air surface. Subsequent analysis of the radar waveform in areas with less expected snow cover showed no resolvable layer in the radargram. However, there was still a significant difference between the heights determined by the laser and the peak radar response. In these cases, the leading edge of the radar waveform contained a small hump that was coincidental with the laser height. The radar was unable to resolve the upper and lower limit of the snow layer, but again a major conclusion was that the radar was more sensitive to the lower snow interface while the laser was sensitive only to the upper snow interface.

[9] These observations and conclusions brought forth the possibility of a new remote sensing technique to produce measurements that could not be achieved by the laser or radar individually [*Leuschen and Raney*, 2006; *Giles et al.*, 2007]. Snow cover could be estimated by comparing the height estimates of coincidental and simultaneous laser and radar altimeters. This type of comparison is presented here using data collected during the 2004 Antarctic AMSR-E Sea Ice field campaign.

3. Field Campaign

[10] In the austral winter of 2003, the NASA P-3 was deployed during the Antarctic AMSR-E Sea Ice (AASI) calibration and validation field campaign. The AMSR-E (EOS Advanced Microwave Scanning Radiometer) instrument aboard the AQUA spacecraft retrieves sea ice concentration using passive radiometric temperature measurements over a variety of microwave frequency bands. Two of the instruments on board the aircraft were the Airborne Topographic Mapper (ATM) laser altimeter and the Delay-Doppler Phase-Monopulse (D2P) radar altimeter. The role of these altimeters during this campaign were to provide precise height measurements from which estimates of sea ice concentration, freeboard, and snow cover could be retrieved. After the first flight, the 2003 campaign had to be postponed because of aircraft mechanical problems. In October 2004, the AASI campaign was resumed on a Naval Research Laboratory (NRL) P-3. Figure 1 shows the flight tracks during both the 2003 (in red) and 2004 (in blue) AASI campaigns. The data presented in this paper were collected on 14 October 2004 and correspond to the dark blue flight track in Figure 1. The background of the image shows the SSM/I derived sea ice concentration. The data collected along the other flight lines are not suitable for comparisons between the laser and radar because either technical problems did not allow position

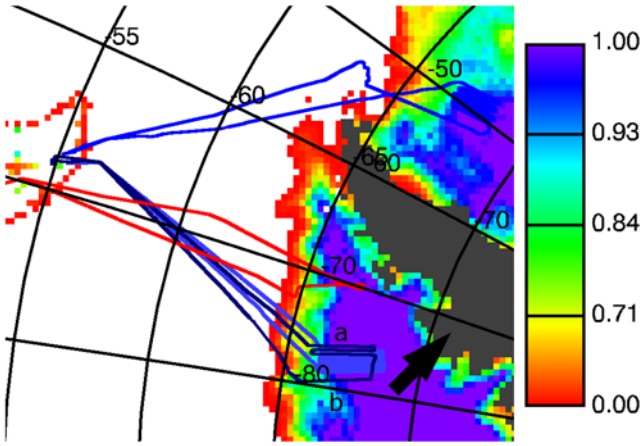

Figure 1. Flight trajectories during AASI 2003 in red and 2004 in blue. The dark blue trajectory with labeled regions a and b corresponds to the presented data. The background image shows the SSM/I derived sea ice concentration with corresponding color bar in the upper right. The black arrow indicates the wind direction during the flights. Wind speed was approximately 10 m s^{-1}.

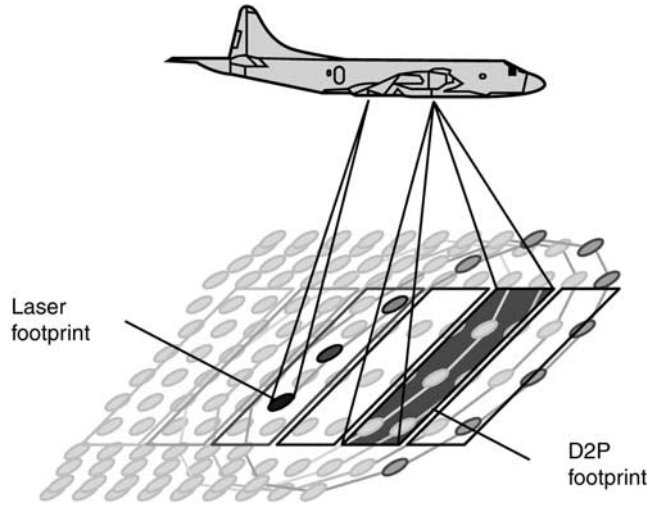

Figure 3. Survey configuration (not to scale). The conical scanning laser footprint is shown as circles, while the radar footprint is shown as a rectangle. The laser swath encompasses the radar footprint.

and altitude measurements or the flight lines were performed at high altitude excluding laser measurements. The measurements are further categorized into two regions, region a and region b, as indicated in Figure 1. The arrow shows the wind direction during the flight on 14 October. Figure 2 shows the air temperature in this region the day of and 2 weeks preceding the measurements.

4. Instrumentation

[11] The primary instrument on board the NRL P-3 was the Polarimeteric Scanning Radiometer (PSR) functioning as the airborne version of AMSR [*Piepmeier and Gasiewski*, 1996]; however, this paper focuses on supporting scientific instrumentation deployed in addition to the PSR. More specifically, two altimeters were also flown to measure the distribution of the sea ice freeboard and snow cover thickness, thus providing the third dimension of the sea ice characteristics.

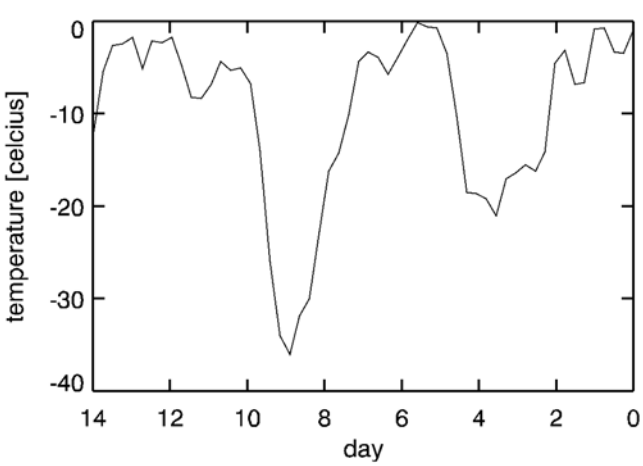

Figure 2. Air temperature in the region where data were collected the day of and 2 weeks preceding the flight. Points are separated by 6-hour periods.

[12] The Airborne Topographic Mapper (ATM) is a laser altimeter that has a long heritage of tracking topographic changes of the Earth's ice cover [*Krabill et al.*, 1999, 2000]. As the PSR is an airborne version of AMSR, the ATM serves as a calibration instrument for the Geoscience Laser Altimeter System (GLAS) on board the Ice, Cloud, and land Elevation Satellite (ICESat) [*Martin et al.*, 2005]. More recently, the ATM has demonstrated the ability to measure certain properties of sea ice, notably its roughness [*Maslanik et al.*, 2006; *Rivas et al.*, 2006]. The ATM is a scanning laser altimeter developed at NASA/Wallops capable of providing three-dimensional digital elevation maps of the sea ice freeboard. The laser shots are collected using a conical scan pattern providing an overlapping circular swath of approximately 120–400 m depending on the aircraft altitude.

[13] The Delay-Doppler Phase-Monopulse (D2P) radar altimeter is an airborne prototype for a new generation of satellite radar altimeters [*Raney and Jensen*, 2001]. The D2P has been previously deployed as a calibration instrument in support of prelaunch activities for the SAR Interferometer Radar Altimeter (SIRAL) on board CryoSat [*Raney and Jensen*, 2002]. In addition to the measurements presented here, the combination of the D2P and ATM has also been used in 2002 during an arctic field campaign and subsequently during a 2006 AMSR-E arctic field campaign, both on board the NASA P-3 platform. Although the D2P and ATM have collected a large amount of sea ice data on other field campaigns, the data and results presented here represent the only flights over Antarctic sea ice in the Bellingshausen Sea.

[14] The measurement geometry of the altimeter instruments deployed on the NRL P-3 is illustrated in Figure 3.

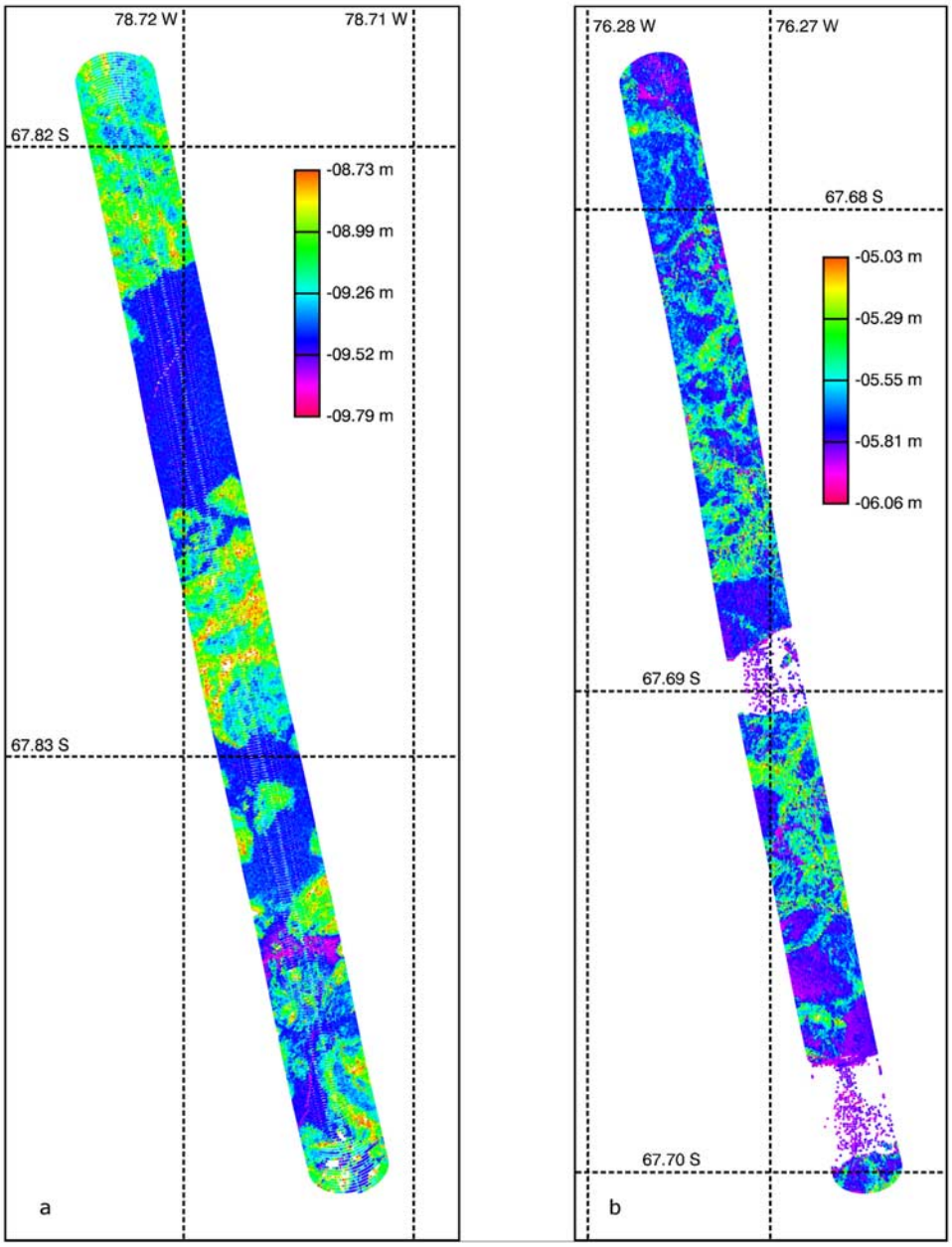

Figure 4. Laser data over sea ice for regions a and b identified in Figure 1. Color bars in the upper right show the corresponding range of height values.

The laser and radar collected coincidental and simultaneous measurements of the sea ice surface topography. The laser collects data in a conical scan pattern producing overlapping circles resulting in fine spatial sampling. The D2P data are coherently processed to produce consecutive footprints that are beam-limited in the along track to around 5 m and pulse-limited footprints in the cross track to around 30 m. The centroid of the radar footprint is at nadir in the along-track direction owing to the coherent processing, and is orthogonal to the slope of the local terrain in cross-track direction. The conical scan of the ATM encompasses the entire D2P footprint with many 1-m-diameter laser shots. The beam width of the radar antenna is four degrees in the along track and eight degrees in the cross track so any data containing a pitch or roll that exceeds approximately two degrees or approximately four degrees, respectively, is discarded to ensure the radar illumination is always at nadir.

5. Calibration

[15] Calibration of the laser and radar altimeters can be classified into two categories, absolute and relative (or cross calibration). Aircraft motion effects must be removed prior to any calibration. The laser and radar are not exactly collocated on the aircraft and, as a result, their relative position changes with the aircraft attitude. The position and altitude of the aircraft are determined from differential GPS and an INS system. The locations of the laser optics, radar antenna, and GPS antenna were all precisely measured in x, y, and z to account for any height variations due to aircraft

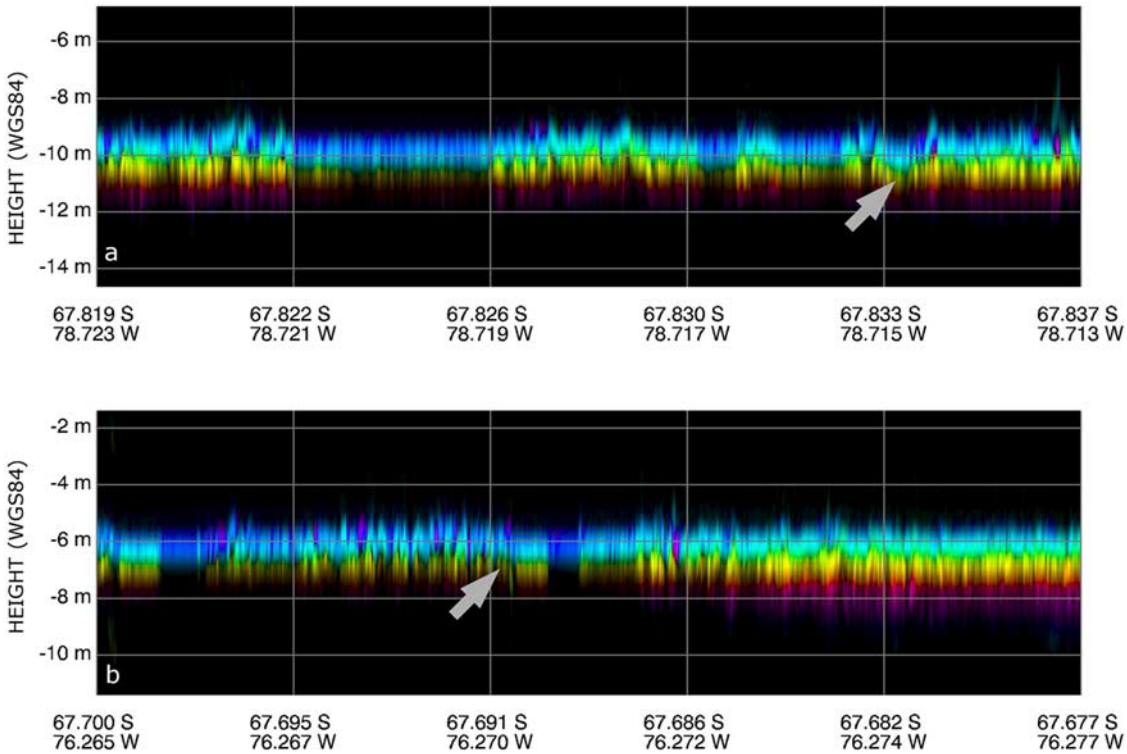

Figure 5. Radargram data over sea ice. Echo power is mapped into the value, and angle of arrival is mapped into the hue of the image. The arrow in Figure 5a shows a region where the radar is lower than sea level, and the arrow in Figure 5b shows a region where the laser is deeper than the radar.

motion, subsequently compensated during postmission processing.

[16] Absolute calibration of the altimeters involves collecting data over a known surface in order to adjust the subsequent heights derived from the field measurements to a common reference datum, in this case the 1984 World Geodetic System (WGS84). This calibration is normally accomplished through overflights of a surveyed aircraft parking area located at NASA's Wallops Flight Facility. The radar system collected data from four passes at different altitudes over the surveyed parking area. The laser was not similarly calibrated premission, owing to schedule constraints. The resulting RMS errors between the runway survey and derived radar heights were on the order of 0.03 m for all four passes.

[17] The instruments are cross calibrated by determining a relative offset such that subsequent offsets can be attributed to differing penetration and reflectivity characteristics of the observed media. Leads within the sea ice provide suitable in situ calibration references, since the top surface of calm open water should give rise to comparable height measurements by both instruments. These observations were sufficient for relative height calibrations of the laser and radar altimeters. Postmission processing of the data yielded a constant calibration offset between the radar and the laser height measurements.

[18] The calibration relied on the identification of areas containing leads from the laser images and radar waveform characteristics. As an example, Figure 4 shows images of laser data collected over leads of open water and newly formed grease ice. The locations for each of these images are indicated in Figure 1 as region a and region b. Open water can be identified by level and flat areas of minimal height. The wind, measured to be $\sim$10 m s^{-1} from reanalysis data for this day, provides sufficient roughness to obtain backscatter off the water surface. In contrast, new "grease" ice can be identified by the regions where laser coverage is sparse, as a result of very low off-nadir backscattered power from the specular surface of the new ice. The open water is consistently downwind of the new ice (wind direction is shown by the black arrow in Figure 1). Cold air blows off the ice, freezes the water just off the ice, and then warms and does not freeze the water downwind. A few similarities and differences can also be identified between the regional characteristics of the sea ice at and around region a and region b. First the range of heights in both regions appears to fluctuate by about 1 m. There is a difference in the absolute height values between the two regions where region a fluctuates around -9.25 m and region b fluctuates around -5.55 m. Finally, the topography appears different as region a tends to contain very distinguishable areas containing leads and plateaus of sea ice and region b tends to vary more with the mean value closer to the height of the leads and containing ridges. These similarities and differences are consistent with all the remaining laser altimeter data in these regions. Additionally, the SSM/I sea ice concentration shows higher concentration in region a than region b.

[19] Figure 5 shows the corresponding radar images for regions a and b. These images are typical radargrams where the y axis represents the radar waveform and the x axis represents location. In these images, the radar power is

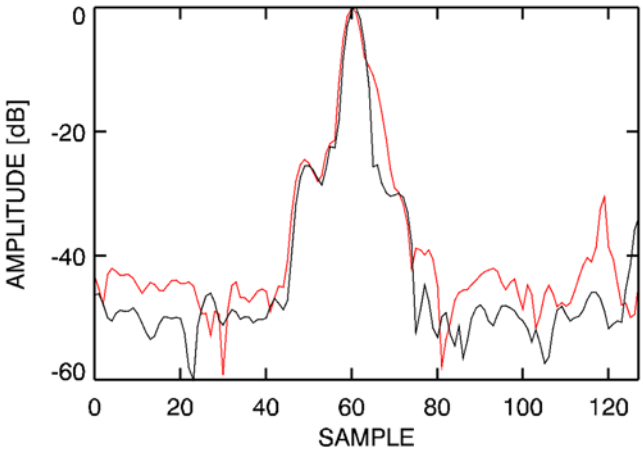

Figure 6. Normalized radar waveform over new "grease" ice in black and open water in red. The waveform over new ice shows a narrower "specular" peak and better signal-to-noise ratio, while the waveform over open water has a slight increase in off-nadir backscatter seen by the hump in the trailing edge of the peak.

mapped into the intensity (or value in a HSV color scheme). In other words, the brighter the color, the more reflected power. The radar makes use of two receive channels in an interferometer configuration designed to measure cross-track surface slope that may occur for land ice sheets. The hue of the radargram represents the cross-channel phase difference, which is used to determine angle of arrival, hence cross-track surface slope. The blue/green/yellow streak running down the center from left to right is the echo from the surface. The regions where the surface is blue represent a single nadir reflection off a smooth surface, and as the surface becomes rougher off-nadir contributions are added mixing the color or hue of the return. Again, areas containing open water leads and new "grease" ice are easily identified. The "blue" specular response of the new ice produces a very large "ideal" peak in the black radar waveform of Figure 6. The waveform shows a single response with range sidelobes on either side. The radar waveform over larger areas of open water shows a slight increase in off-nadir backscatter (more colors in the radargram) and a reduction in peak signal amplitude (with respect to the new ice waveform) due to larger wind-driven surface roughness as shown in red in Figure 6. Radar waveforms over snow and ice show a decrease in peak signal power and a more prominent decay due to enhanced off-nadir backscatter. These characteristics make it easy to identify the necessary calibration leads.

[20] A total of 1200 measurement locations over leads from within the entire data set were analyzed. Figure 7a shows the offset, laser height minus radar height, for each of these 1200 samples, and Figure 7b shows the distribution as having a mean of −0.78 m and a standard deviation of 0.05 m. The −0.78-m offset is determined as the cross-calibration offset between the laser and the radar, while also providing an absolute offset for the laser. The value of −0.78 m has a 99% confidence range of less than 0.01 m for 1200 samples and a 0.05-m standard deviation. The standard deviation of 0.05 m also suggests that any deviation greater than this value for comparisons over sea ice is due to the geophysical nature of the snow and ice rather than instrument offsets.

6. Laser-Radar Comparisons

[21] Figure 8 shows a comparison of laser and radar data collected over Antarctic sea ice. This is the same laser data as shown in Figure 4a overlain with the radar height values derived from the data in Figure 5a and mapped into appropriate radar footprint locations and sizes. The radar heights were obtained by finely resampling the radar waveforms and tracking the halfway point on the leading edge of the peak echo. As illustrated in the image, the location of the radar footprint over the leads remains constant in the cross-track direction owing to the lack of surface slope. The effective centroid of the radar footprint in the cross track wanders over the rougher sea ice, essentially following the locus of surface features that are at minimum range with respect to the radar. To the first order, the laser and radar measurements coincide very well, both tracking the same

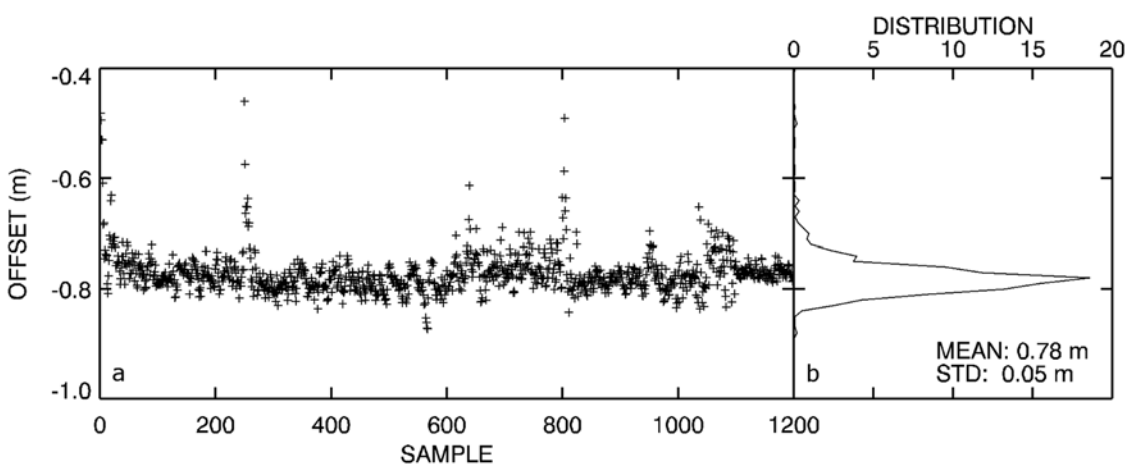

Figure 7. Lead data used to cross calibrate the laser and radar altimeters. (a) Height offset (laser minus radar) for 1200 samples over leads. (b) Distribution showing a mean value of −0.78 m and a standard deviation of 0.05 m.

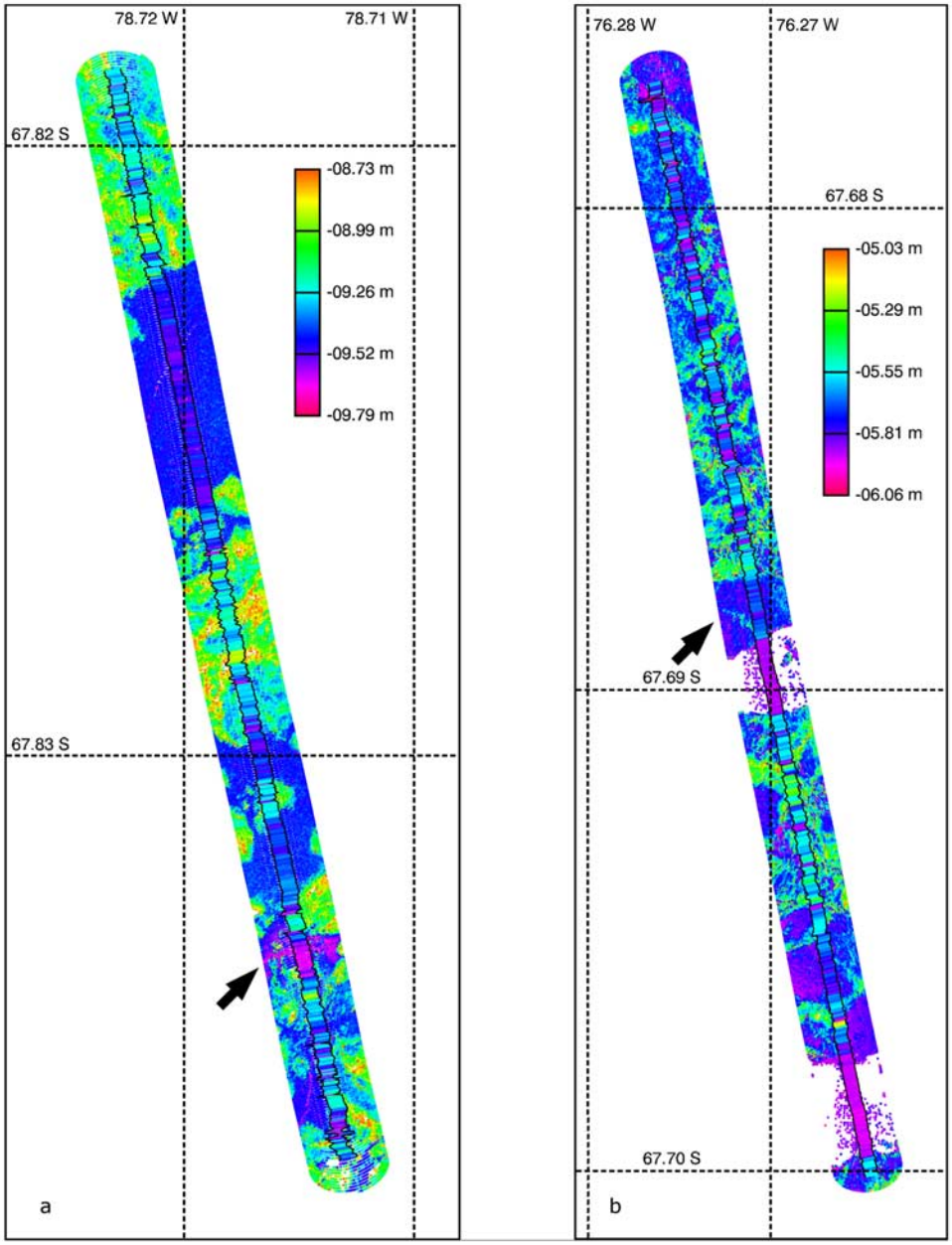

Figure 8. Image of radar estimated height values overlain on the laser elevation map. The arrow in Figure 8a shows a region where the radar is lower than sea level, and the arrow in Figure 8b shows a region where the laser is deeper than the radar.

features of sea ice, leads, and ridges. Fine-scale differences are difficult to interpret using this type of comparison.

[22] Choice of the radar tracking algorithm and threshold may bias the comparisons with the laser. The actual track point of the radar waveform generated over the lead could be significantly different than that of the waveform generated over the sea ice depending on the surface roughness. A rougher sea ice surface may produce a waveform with a significantly longer rising edge, thus introducing a height estimation bias that is dependent on the surface roughness characteristics. Such waveform deformation is difficult to differentiate from penetration effects. Figure 9 shows a comparison of radar heights using tracking thresholds of 50 percent and 90 percent of the peak value for the two regions a and b. The mean offset between the two tracking thresholds is less than 0.01 m with a 0.02-m standard deviation. These offsets are smaller than the offset between the laser and radar as subsequently discussed.

[23] The surface illuminations of the two instruments differ, 1-m circle for the laser and a 5-m by 30-m area for the radar. Quantitative comparisons of laser and radar data require the measurement footprints be comparable after suitable data selection and processing. As illustrated in Figure 3 and Figure 8, the laser scan swath fully encompasses the radar footprints with many 1-m "point" measurements. Therefore, our analysis only uses that subset of the laser measurements that coincide with the radar's footprint. The qualifying laser data are averaged over the radar

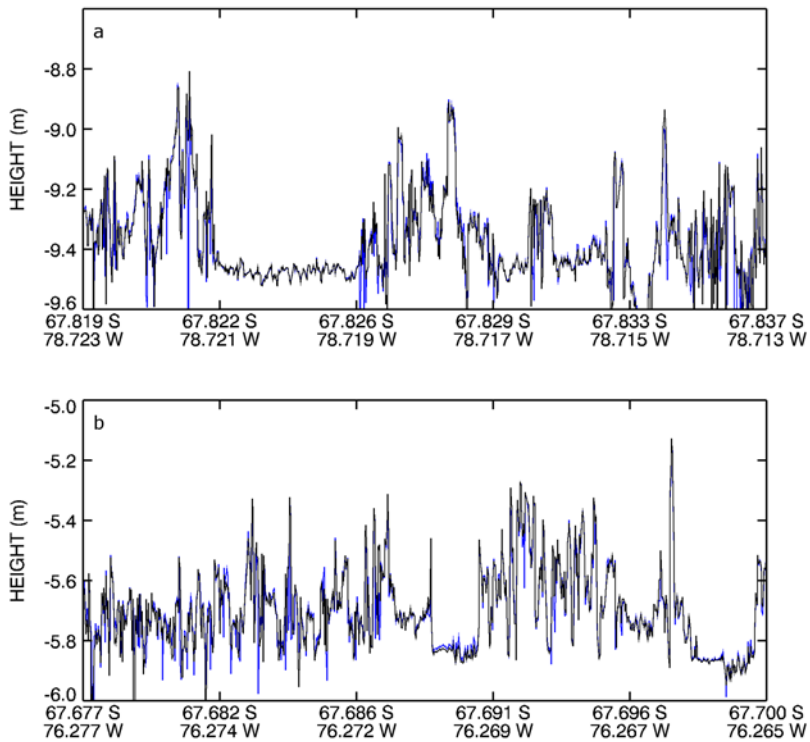

Figure 9. Comparison of 50 percent (black) and 90 percent (blue) tracking for radar height tracking.

footprint, weighted by the cross-track antenna pattern of the radar. Thus, this methodology assures that the effective height measurements of the two instruments are derived from the same area.

[24] Figure 10 shows a comparison of the radar heights and the averaged laser heights for the two regions a and b. The data points from both plots relate to the same footprint size and location on the sea ice. Again, the correlation of the two measurements over large-scale features is good. The shapes of the peaks, edges, and leads all match, aside from high-frequency variations and low-frequency mean offsets. The comparison over the leads shows no offset and the correlation is excellent. Over the sea ice, the laser height is generally higher than that of the radar and more high-frequency variations are apparent. Data from the middle of Figure 10a suggest that the snow surface is smoother than the rougher ice surface. This is typical of deformed sea ice where snow drifts accumulate between the ridges, often asymmetrically downwind of the ridge. The locations where the laser height is higher than the radar can be explained as the radar penetrating a layer of snow cover and reflecting off the underlying ice, while the laser reflects from the snow's top surface. Thus, the difference between the laser and radar is a measure of snow cover thickness.

[25] There are other features that are more challenging to explain. These features include areas where the radar height is lower than expected sea level and also where the laser appears lower than the radar. An example of the suspect regions where the radar is lower than sea level is illustrated near 67.833S, 78.715W and identified by the arrows in Figures 5a, 8a, and 10a. These areas do not exhibit waveform characteristics typical of water or new ice leads and are not classified as such. They also occur when there is a corresponding peak in the laser height. This minimum radar height and local maximum laser height could be inferred as a relatively thick layer of snow cover, thus loading the ice below sea level. The regions where the surface detected by the laser is lower than that detected by the radar are more difficult to explain and with the limitations of the collected data can only be speculated upon. An example can be seen near the center of Figures 5b, 8b, and 10b (again identified by arrows). One plausible explanation is that the laser is actually penetrating a clear water pond on an ice floe. Such water would be transparent to the laser, but would provide a reflecting surface for the radar. Regions where the laser is lower than the radar seem to be more prominent in region b of Figure 1, an area that appears to consist of many ice floes with raised edges and water in the middle on the basis of the laser topography.

7. Results

[26] Figure 11 shows a scatterplot containing all laser and radar height estimates. The green data points correspond to region a and the blue data points correspond to region b. The solid black line identifies locations where radar and laser heights are equal and intersects the mean offset between the lead data used in calibration. All points to the left of the black line correspond to measurement locations where the laser height is greater than that of the radar, and points to the right correspond to measurement locations where the radar height is greater than the laser. The two clusters represent data from the different areas surveyed; the offset between the clusters represents a difference in sea level mainly due to changes in the geoid and tides. However, it is not the absolute position along the black line that

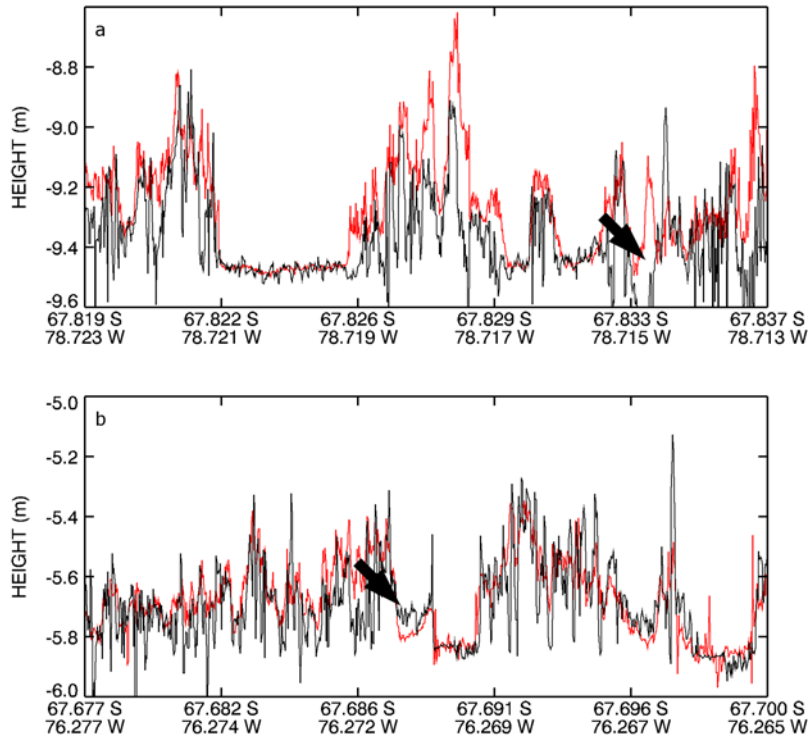

Figure 10. Comparison of radar (black) tracking height and laser (red) heights mapped into corresponding radar footprints. The arrow in Figure 10a shows a region where the radar is lower than sea level, and the arrow in Figure 10b shows a region where the laser is deeper than the radar.

is important, but rather the distance from the line that represents an offset.

[27] Figure 12 shows the distribution of laser minus radar offsets for all measurement locations. Again, the green plot is for region a, the blue plot is for region b, and the black plot is for both. This distribution is a significant result of these data, and shows the level of penetration of the radar pulse into the snow cover and sea ice compared to the laser. This penetration provides an indication of snow cover thickness. The most frequent or mode value of all the measurement locations aligns exactly (within 0.01 m) with the mean offset value of the lead locations, showing that the radar and laser measure the same height most of the time. The mean value of the distribution is positive and has a value of 0.1 m. The distribution for region a shows more snow cover than region b by about 0.05–0.1 m.

8. Discussion

[28] This paper provides measurements of simultaneous and coincidental airborne laser and radar altimeters over Antarctic sea ice. The differences between the height

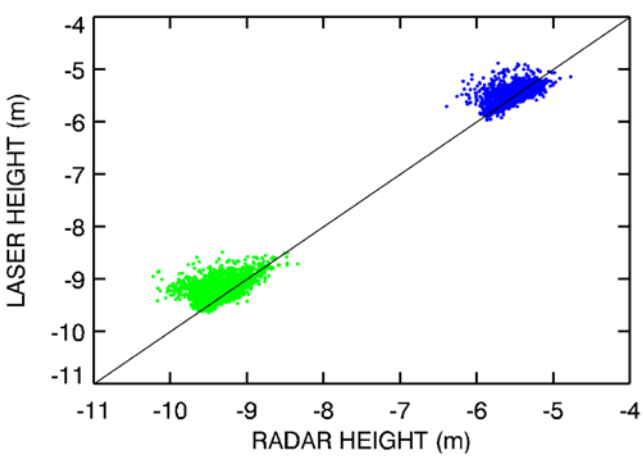

Figure 11. Scatterplot of all laser and radar height estimates. Green points refer to region a and the blue points refer to region b.

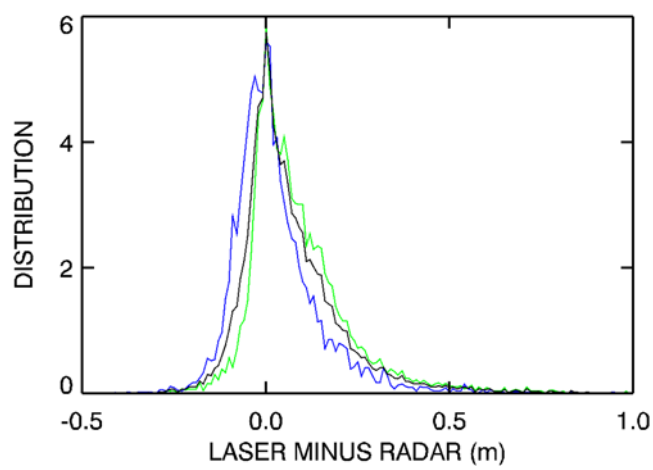

Figure 12. Histogram of laser minus radar offset for all measurement locations. Green line refers to region a, blue line refers to region b, and the black line refers to all points.

measurements of the two instruments provides a means of estimating snow cover, a parameter that has been difficult to obtain over long survey distances. Snow cover is a very important value when trying to determine sea ice thickness from laser altimetry, such as measurements from ICESat/GLAS. We found that the estimated snow cover has a mean value of approximately 0.1 m and ranges from zero to around a meter or more over the regions we observed. Owing to the remote nature of the survey, there are no coincidental in situ measurements to confirm these conclusions. However, the distribution does match the expected values determined from previous in situ measurements in these regions [*Massom et al.*, 2001].

[29] The purpose of this paper is to show a reasonable plausibility that the utilization of coordinated laser and radar sensors can perhaps resolve the ambiguity of snow cover, and therefore lead to improved sea ice thickness measurements. In at least part of the study region, the results are reasonable and clearly demonstrate that the use of concurrent radar and laser altimeter measurements to measure the snow thickness is a very viable option. In other regions, there appears to be some inconsistencies in that the surface detected by the laser is lower than that detected by the radar. This dilemma can be resolved if our hypothesis about the presence of surface water on ice floes with raised edges in these regions is correct. This study thus suggests that there may be regions within the ice pack where the joint system may not produce correct snow thickness. However, it may be used to detect these special types of sea ice cover, the areal coverage of which is likely of interest to the scientific community because of their potential impact on heat and moisture flux calculations.

References

Aagaard, K., and E. C. Carmack (1989), The role of sea ice and other fresh water in the Arctic circulation, *J. Geophys. Res.*, *94*, 14,485–14,498.

Beaven, S. G., G. L. Lockhart, S. P. Gogineni, and A. R. Hosseinmostafa (1995), Laboratory measurements of radar backscatter from bare and snow-covered saline ice sheets, *Int. J. Remote Sens.*, *16*, 851–876.

Cavalieri, D. J., C. L. Parkinson, and K. Y. Vinnokov (2003), 30-year satellite record reveals contrasting Arctic and Antarctic decadal sea ice variability, *Geophys. Res. Lett.*, *30*(18), 1970, doi:10.1029/2003GL018031.

Comiso, J. C. (2002), A rapidly declining perennial sea ice cover in the Arctic, *Geophys. Res. Lett.*, *29*(20), 1956, doi:10.1029/2002GL015650.

Curry, J. A., J. L. Schramm, and E. E. Ebert (1995), Sea ice-albedo climate feedback mechanism, *J. Clim.*, *8*, 240–247.

Fichefet, T., and M. A. Morales Maqueda (1999), Modeling the influence of snow accumulation and snow-ice formation on the seasonal cycle of the Antarctic sea-ice cover, *Clim. Dyn.*, *15*, 251–268.

Giles, K. A., et al. (2007), Combined airborne laser and radar altimeter measurements over the Fram Strait in May 2002, *Remote Sens. Environ.*, *111*, 135–408.

Gosselin, M., M. Levasseur, P. A. Wheeler, R. A. Horner, and B. C. Booth (1997), New measurements of phytoplankton and ice algal production in the Arctic Ocean, *Deep Sea Res., Part II*, *44*, 1623–1644.

Krabill, W., E. Frederick, S. Manizade, C. Martin, J. Sonntag, R. Swift, R. Thomas, W. Wright, and J. Yungel (1999), Rapid thinning of parts of the southern Greenland ice sheet, *Science*, *283*, 1522–1524.

Krabill, W., W. Abdalati, E. Frederick, S. Manizade, C. Martin, J. Sonntag, R. Swift, R. Thomas, W. Wright, and J. Yungel (2000), Greenland ice sheet: High elevation balance and peripheral thinning, *Science*, *289*, 428–430.

Kwok, R., E. Rignot, B. Holt, and R. Onstott (1992), Identification of sea ice types in spaceborne synthetic aperture radar data, *J. Geophys. Res.*, *97*, 2391–2402.

Kwok, R., H. J. Zwally, and D. Yi (2004), ICESat observations of Arctic sea ice: A first look, *Geophys. Res. Lett.*, *31*, L16401, doi:10.1029/2004GL020309.

Laxon, S., N. Peacock, and D. Smith (2003), High interannual variability of sea ice thickness in the Arctic region, *Nature*, *425*, 947–950.

Leuschen, C. J., and R. K. Raney (2006), Initial results of data collected by the JHU/APL D2P radar altimeter over land- and sea-ice, *Johns Hopkins APL Tech. Dig.*, *26*, 114–122.

Lindsay, R. W., and D. A. Rothrock (1995), Arctic sea ice leads from advanced very high resolution radiometer images, *J. Geophys. Res.*, *100*, 4533–4544.

Martin, C., R. Thomas, W. Krabill, and S. Manizade (2005), ICESat range and mounting bias estimation over precisely-surveyed terrain, *Geophys. Res. Lett.*, *32*, L21S07, doi:10.1029/2005GL023800.

Maslanik, J., et al. (2006), Spatial variability of barrow-area shore-fast sea ice and its relationships to passive microwave emissivity, *IEEE Trans. Geosci. Remote Sens.*, *44*(11), 3021–3031.

Massom, R. A., et al. (2001), Snow on Antarctic sea ice, *Rev. Geophys.*, *39*, 413–445.

Nolin, A. W., F. M. Fetterer, and T. A. Scambos (2002), Surface roughness characterizations of sea ice and ice sheets: Case studies with MISR data, *IEEE Trans. Geosci. Remote Sens.*, *40*(7), 1605–1615.

Piepmeier, J. R., and A. J. Gasiewski (1996), Polarimetric scanning radiometer for airborne microwave imaging studies, *Proc. IEEE Int. Geosci. Remote Sens. Symp.*, *2*, 1120–1122.

Powell, D. C., T. Markus, and A. Stössel (2005), The effects of snow depth forcing of Southern Ocean sea ice simulations, *J. Geophys. Res.*, *110*, C06001, doi:10.1029/2003JC002212.

Rahmstorf, S. (1997), Risk of sea-change in the Atlantic, *Nature*, *338*, 825–826.

Raney, R. K., and J. R. Jensen (2001), The new generation of radar altimeters: Proof of concept, *Rep. SRO-01-16*, Appl. Phys. Lab., Johns Hopkins Univ., Laurel, Md.

Raney, R. K., and J. R. Jensen (2002), An airborne CryoSat prototype: The D2P radar altimeter, *Proc. IEEE Int. Geosci. Remote Sens. Symp.*, *3*, 1765–1767.

Raney, R. K., and C. J. Leuschen (2003), Technical support for the deployment of radar and laser altimeters during LaRA 2002, *Rep. SRO-03M-09*, Appl. Phys. Lab., Johns Hopkins Univ., Laurel, Md.

Raney, K., C. J. Leuschen, R. D. Chapman, J. R. Jensen, and B. L. Gotwols (2003), LaRA-2002: Results of the airborne laser and radar altimeter campaign over Greenland, Svalbard, and Arctic sea ice, *Proc. IEEE Int. Geosci. Remote Sens. Symp.*, *7*, 4392–4394.

Rignot, E., K. Echelmeyer, and W. Krabill (2001), Penetration depth of interferometric synthetic-aperture radar signals in snow and ice, *Geophys. Res. Lett.*, *28*, 3501–3504.

Rivas, M., J. Maslanik, J. Sonntag, and P. Axelrad (2006), Sea ice roughness from airborne LIDAR profiles, *IEEE Trans. Geosci. Remote Sens.*, *44*(11), 3032–3037.

Smetacek, V., and S. Nicol (2005), Polar ocean ecosystems in a changing world, *Nature*, *437*, 362–368.

Wheeler, P. A., M. Gosselin, E. Sherr, D. Thibault, D. L. Kirchman, R. Benner, and T. E. Whitledge (1996), Active cycling of organic carbon in the central Arctic Ocean, *Nature*, *380*, 697–699.

Wu, X., W. F. Budd, V. I. Lytle, and R. A. Massom (1999), The effects of snow on Antarctic sea ice simulations in a coupled atmosphere-sea ice model, *Clim. Dyn.*, *15*, 127–143.

R. D. Chapman and R. K. Raney, Applied Physics Laboratory, Johns Hopkins University, 11100 Johns Hopkins Road, Laurel, MD 20723-6099, USA.

J. C. Comiso, Cryospheric Sciences Branch, NASA Goddard Space Flight Center, Code 614.1, Greenbelt, MD 20771, USA.

W. B. Krabill, J. G. Sonntag, and R. N. Swift, Observational Science Branch, NASA Goddard Space Flight Center, Wallops Island, VA 23337, USA.

C. J. Leuschen, Center for Remote Sensing of Ice Sheets, University of Kansas, 2335 Irving Hill Road, Lawrence, KS 66045, USA. (leuschen@eecs.ku.edu)